Clim. Past Discuss., 8, 2731–2776, 2012
www.clim-past-discuss.net/8/2731/2012/
doi:10.5194/cpd-8-2731-2012

Climate of the Past Discussions

Quantification of the Greenland ice sheet contribution to Last Interglacial sea-level rise

E. J. Stone[1], D. J. Lunt[1], J. D. Annan[2], and J. C. Hargreaves[2]

[1]BRIDGE, School of Geographical Sciences, University of Bristol, Bristol, UK
[2]Research Institute for Global Change, JAMSTEC, Yokohama, Japan

Received: 2 July 2012 – Accepted: 9 July 2012 – Published: 20 July 2012

Correspondence to: E. J. Stone (emma.j.stone@bristol.ac.uk)

Published by Copernicus Publications on behalf of the European Geosciences Union.

Abstract

The Last Interglaciation (∼130–115 thousand years ago) was a time when the Arctic climate was warmer than today (Anderson et al., 2006; Kaspar et al., 2005) and sea-level extremely likely at least 6 m higher (Kopp et al., 2009). However, there is large uncertainty in the relative contributions to this sea-level rise from the Greenland and Antarctic ice sheets and smaller icefields (Otto-Bliesner et al., 2006; Huybrechts, 2002; Letréguilly et al., 1991; Ritz et al., 1997; Cuffey and Marshall, 2000; Tarasov and Peltier, 2003; Lhomme et al., 2005; Greve, 2005; Robinson et al., 2011; Fyke et al., 2011). By performing an ensemble of 500 coupled climate – ice sheet model simulations, constrained by paleo-data, we determine probabilistically the likely contribution of Greenland ice sheet melt to Last Interglacial sea-level rise, taking into account model uncertainty. Here we show a 90 % probability that Greenland ice melt contributed at least 0.6 m but less than 10 % probability it exceeded 3.5 m, a value which is lower than several recent estimates (Cuffey and Marshall, 2000; Tarasov and Peltier, 2003; Lhomme et al., 2005; Robinson et al., 2011). Our combined modelling and paleo-data approach suggests that the Greenland ice sheet is less sensitive to orbital forcing than previously thought, and implicates Antarctic melt as providing a substantial contribution to Last Interglacial sea-level rise.

1 Introduction

Past time periods provide important case studies for evaluating the performance of Earth system models, since model results can be compared with geological records. In particular, warm climates of the past are useful as they can also provide an analogue for possible future warming. The Last Interglaciation (LIG) provides such a case study as globally averaged sea-level was thought to be several metres higher than today, and high latitude temperatures warmer. Estimates of maximum sea-level increase, derived from sedimentary deposits and coral sequences, typically range from 4 to 6 m (Muhs et al., 2002; Rostami et al., 2000). A recent sea-level data synthesis shows that sea-level was likely up to 8 m higher than today with the highstand extremely likely (95 % probability) greater than 6 m (Kopp et al., 2009), consistent with less glacial ice on Earth during the LIG. The likely contributors to the sea-level rise are ice losses from the Greenland and Antarctic ice sheets along with high latitude Arctic icefields such as those in the Canadian Arctic, together with thermal expansion of sea-water.

Further evidence from proxy data located in the Arctic and European regions suggests the LIG climate featured temperatures, at least regionally, several degrees warmer than today (Anderson et al., 2006; Kaspar et al., 2005). This is supported by climate model simulations indicating summer Arctic warming was as much as 5 °C relative to modern, with the greatest warming over Eurasia and in the Baffin Island/Greenland region (Kaspar et al., 2005; Montoya et al., 2000; Otto-Bliesner et al., 2006). Paleo pollen, macrofossil and soil records suggest the expansion of boreal forests northwards into areas now occupied by tundra in Russia, Siberia and Alaska during peak LIG warmth (Muhs et al., 2001; Kienast et al., 2008). On Greenland itself, ice core measurements from the Summit region indicate ice was present throughout the LIG, with the surface elevation no more than a few hundred metres lower than present day based on the total gas content of the ice (Raynaud et al., 1997). Estimates of the Greenland ice sheet (GrIS) contribution to sea-level rise during the LIG range from 0.4 to 5.5 m based on paleothermometry from ice cores coupled with thermo-dynamical ice sheet models (Huybrechts, 2002; Letréguilly et al., 1991; Ritz et al., 1997; Cuffey and Marshall, 2000; Tarasov and Peltier, 2003; Lhomme et al., 2005; Greve, 2005) and coupled climate-ice sheet models of varying complexity (Robinson et al., 2011; Fyke et al., 2011; Otto-Bliesner et al., 2006).

Here we assess the contribution of Greenland ice loss to global sea-level rise, derived from simulations of the LIG global climate and evolution of the GrIS from 130 to 120 ka using the general circulation model (GCM) HadCM3 coupled to the ice sheet model Glimmer over the Greenland region using an efficient offline coupling methodology to account for ice sheet climate interactions (DeConto and Pollard, 2003).

2 Model description

2.1 The climate model

The GCM simulations described in this paper are carried out using the UK Met Office coupled atmosphere-ocean GCM, HadCM3, version 4.5 (Gordon et al., 2000). The atmosphere component of HadCM3 is a global grid-point hydrostatic primitive equation model, with a horizontal grid-spacing of 2.5° (latitude) by 3.75° (longitude) (73 by 96 grid points) and 19 levels in the vertical with a time step of 30 min. The performance of the atmosphere component is described in Pope et al. (2000) where HadAM3 (the atmosphere only version of the Hadley Centre Model) is run with observed sea surface temperatures. It has been shown to agree well with observations (Pope et al., 2000). The land surface scheme (MOSES 2), which includes representation of the freezing and melting of soil moisture and the formulation of evaporation, incorporates the dependence of stomatal resistance on temperature, vapour pressure and CO_2. In addition, it treats sub-grid land cover explicitly. Within this land surface scheme ice sheets are prescribed and are fixed. The radiation scheme is that of Edwards and Slingo (1996) with six and eight spectral bands in the shortwave and longwave, respectively. The convective scheme is based on Gregory and Rowntree (1990) with an additional parameterisation of the direct impact of convection on momentum (Gregory et al., 1997). The cloud scheme employed is a prognostic one that diagnoses cloud amount, cloud ice and cloud water based on the total moisture and the liquid water potential temperature. The orography of Greenland is particularly important when considering the deglaciation and reglaciation of the GrIS since previous work has shown it can have profound effects on atmospheric circulation patterns if the ice sheet were removed (Petersen et al., 2004; Junge et al., 2005) since orographic gravity waves represent a major sink of momentum flux in the atmosphere. In order to include the effect of orographic forcing on atmospheric circulation, HadCM3 also includes a parameterisation of orographic drag (Milton and Wilson, 1996) and a gravity wave drag scheme in order to represent the mechanisms of sub-grid scale orographic forcing in stable and

CPD
8, 2731–2776, 2012

turbulent atmospheric flow. The scheme includes anisotropy of orography, high drag states and flow blocking as well as trapped lee waves (Gregory et al., 1998).

The resolution of the ocean model is 1.25° by 1.25° with 20 levels in the vertical. The ocean model uses the mixing scheme of Gent and McWilliams (1990) with no explicit horizontal tracer diffusion. The horizontal resolution allows the use of a smaller coefficient of horizontal momentum viscosity leading to an improved simulation of ocean velocities. The sea-ice model uses a simple thermodynamic scheme and contains parameterisations of ice concentration (Hibler, 1979) and ice drift and leads (Cattle and Crossley, 1995). Surface temperatures and fluxes over the sea-ice and leads fractions of gridboxes are calculated separately in the atmosphere component of HadCM3. The surface albedo of sea-ice is 0.8 at temperatures less than −10 °C and decreases linearly to 0.5 between −10 and 0 °C. This is to account for the aging of snow, formation of melt ponds and the relatively low albedo of bare ice. In simulations of the present-day climate, the model has been shown to simulate sea surface temperatures in good agreement with modern observations, without the need for flux corrections (Gregory and Mitchell, 1997).

2.2 The ice sheet model

We also use the three dimensional thermomechanical ice sheet model Glimmer version 1.0.4 (Rutt et al., 2009). The core of the model is based on the ice sheet model described by Payne (1999). The ice dynamics are represented with the widely-used shallow-ice approximation, and a full three-dimensional thermodynamic model is used to determine the ice flow law parameter. The model is formulated on a Cartesian grid, and takes as input the surface mass-balance and air temperature at each time step. In the present work, the ice dynamics time step is one year. The surface mass-balance is simulated using the positive degree day (PDD) approach described by Reeh (1991). The basis of the PDD method is the assumption that the melt that takes place at the surface of the ice sheet is proportional to the time-integrated temperature above freezing point, known as the positive degree day. The method described by Reeh (1991) and implemented here is somewhat more sophisticated, in that two PDD factors are used, one each for snow and ice, to take account of the different albedos and densities of these materials. The use of PDD mass-balance models is well-established in coupled atmosphere-ice sheet paleoclimate modelling studies (DeConto and Pollard, 2003; Lunt et al., 2008, 2009). Glimmer also includes a representation of the isostatic response of the lithosphere, which is assumed to behave elastically, based on the model of Lambeck and Nakiboglu (1980). The forcing data from HadCM3 are transformed onto the ice model grid using bilinear interpolation, which ensures that precipitation is conserved in the atmosphere-ice sheet coupling. In the case of the surface air temperature field, a vertical lapse-rate correction is used to take account of the difference between the high-resolution topography seen within Glimmer, and that represented within HadCM3. The use of a lapse-rate correction to better represent the local temperature is established in previous work (Pollard and Thompson, 1997; Vizcaíno et al., 2008).

For the baseline climate to which the GCM temperature and precipitation anomalies are applied we use those described in Stone et al. (2010). The temperature climatology are derived from ERA-40 observations (Hanna et al., 2005) and precipitation also from ERA-40 reanalysis (Uppala et al., 2005). The Glimmer ice sheet model uses a single value for the lapse-rate correction which is a tuneable parameter. We use the Greenland bedrock topography of Bamber et al. (2001) on a 20 km resolution grid.

Several parameters in large-scale ice sheet modelling are still poorly constrained, resulting in highly variable ice sheet volume and extent depending on the values prescribed in the model (Ritz et al., 1997). Previous work (Stone et al., 2010) investigated the sensitivity of ice sheet evolution for the modern GrIS to five tuneable parameters which affect the ice sheet dynamics and surface mass balance. These are the PDD factors for ice and snow, near-surface lapse rate, flow enhancing factor and the geothermal heat flux (see Table 1). Here we generate an ensemble of 500 simulations using the method of Latin Hypercube Sampling (LHS) in order to efficiently sample the five

CPD
8, 2731–2776, 2012

dimensional parameter space. This is illustrated in Fig. 1. For more details refer to Stone et al. (2010).

3 Experimental design and coupling methodology

GCM simulations representing 130, 125 and 120 ka are forced with insolation anomalies resulting from changes in the Earth's orbital parameters for the early to mid part of the LIG. Compared with pre-industrial, larger eccentricity and obliquity and Northern Hemisphere summer (as opposed to winter) occurring at perihelion (see Table 2), results in greater seasonality, leading to pronounced high northern latitude summer insolation, consistent with warming observed in the geological record (Anderson et al., 2006; Andersen et al., 2004; Kaspar et al., 2005) (see Fig. 2). This seasonal variation in insolation is important because ice sheet surface mass balance is particularly sensitive to summer warming.

The three LIG snapshot time-slices are run for 100 model years (70 yr spin-up and 30 yr for averaging) with the following Greenland boundary conditions:

1. Modern day GrIS present

2. Partial GrIS present derived from a tuned ice model experiment forced with a 560 ppmv climate (Stone et al., 2010)

3. No GrIS present

This gives a range of climate between which the "expected" climate over a partially melted GrIS during the LIG might lie. One caveat of these climate simulations concerns the use of an isostatic equilibrium for the orography in the ice-free state. Obviously, if there was a substantial ice sheet present before the start of the LIG, as inferred from the eustatic sea-level curve (Siddall et al., 2007), there would likely have been insufficient time for all the ice to melt, the bedrock to rebound fully and soil to develop on the bare rock surface. However, this provides the most contrasting climate scenario to a fully glaciated Greenland being present throughout the LIG (which is also unlikely).

For the LIG the changed forcings from present day are: the modified trace gas concentrations and the seasonal and latitudinal insolation changes at the top of the atmosphere associated with the Milankovitch orbital forcing (Milankovitch, 1941) consistent with the perturbed forcings in the standard PMIP LIG simulations. Figure 2a shows the variation in insolation from 140 to 110 ka for the spring and summer months at three latitudes over Greenland: 65° N, 74° N and 80° N. Insolation anomalies over Greenland relative to present day (Fig. 2b) are at a maximum at ~ 130 ka for May and June and decrease toward 120 ka. Smaller anomalies for July and August peak from ~ 120 to 125 ka. Orbital parameters are taken from Berger and Loutre (1991) for the three time snapshots at 130, 125 and 120 ka. Table 2 shows the obliquity, eccentricity and perihelion for these three scenarios. A further HadCM3 experiment at 136 ka is also included in order to spin-up the ice sheet model sufficiently but differs slightly by including a MOSES 1 land surface scheme (Cox et al., 1999). This simulation is run for 500 model years with an averaging time of 30 yr.

An additional simulation, the pre-industrial control, includes trace gas concentrations (280 ppmv for CO_2, 760 ppbv for CH_4 and 270 ppbv for N_2O) and orbital parameters (obliquity 23.45°, perihelion 2.6 (day of the year) and eccentricity 0.01724) appropriate for 1850 AD.

Also shown in Fig. 2 is the atmospheric CO_2 concentration, reconstructed from ice cores, from 140 to 110 ka based on Luthi et al. (2008). All CO_2 values are on the EDC3 gas age scale (Loulergue et al., 2007). There is a sharp rise in CO_2 concentration between 140 ka and 130 ka from ~ 200 to 260 ppmv. Thereafter, this trace gas concentration stabilises between 260 and 290 ppmv. Since the greenhouse gases do not markedly vary from pre-industrial during the LIG (Luthi et al., 2008) and it has been shown that climate perturbations were predominantly orbitally driven at this time (Slowey et al., 1996; Loutre et al., 2007; Yin and Berger, 2012), gas concentrations are held constant and unchanged from the values used in the pre-industrial simulations.

CPD
8, 2731–2776, 2012

In this way any changes in LIG climate from the pre-industrial are due to changes in the orbital parameters of the Earth. CO_2 is, therefore, held constant at 280 ppmv for all experiments performed using HadCM3 between 130 and 120 ka. All other trace gases are equivalent to pre-industrial values. The exception is for the simulation at 136 ka where CO_2, methane (CH_4) and nitrous oxide (N_2O) are lower compared with pre-industrial at 200 ppmv, 413 ppbv and 229 ppbv, respectively. This is because differences in the trace gases compared with pre-industrial are the driving mechanism for this earlier perturbed climate rather than changes in the orbital parameters compared with pre-industrial (see Fig. 2b where summer high latitude insolation anomalies are small at 136 ka).

Outside of Greenland, global vegetation coverage is prescribed at present-day distributions. The simulations where the GrIS is removed/partially melted are prescribed bare soil coverage in place of Greenland ice while the simulations with a full GrIS included use the present-day ice sheet mask with bare soil in ice-free regions. For the LIG simulations with the ice sheet removed, the bedrock is rebounded and in isostatic equilibrium. Likewise, the simulations with the GrIS included use modern day topography and those with a partial ice sheet use their associated topography. Finally, the land-sea mask remains unchanged from modern since there were no significant tectonic changes to the continents between 130 ka and present and the estimated sea-level change would result in negligible land-sea mask changes.

All GCM simulations were continued from pre-industrial simulations of 100 model years with the appropriated bedrock and ice coverage. Figure 3 shows the average temperature evolution over Greenland (one of the inputs into the Glimmer ice sheet model) including this pre-industrial spin-up. A 10-yr running average (red) and 10-yr mean trend (blue) are shown and indicate sufficient spin-up of the model near-surface temperature in response to the changed orbits. They show that compared with inter-annual variability the simulations are close to equilibrium.

It is not known exactly how big the GrIS was at 130 ka (or at any other point during the LIG), although sea-level was similar to present day (Siddall et al., 2007; Kopp et al.,

CPD
8, 2731–2776, 2012

2009) implying a substantial amount of ice must have been present at high northern and southern latitudes. Since it is not practically possible to spin-up an ensemble of coupled HadCM3 ice sheet model configurations for several glacial-interglacial cycles, an approach is used that assumes the ice sheet is in equilibrium at the start of the transient ice sheet model simulations. In order that changes in the ice sheet response to climate at 130 ka are not a result of inadequate spin-up of the ice sheet model, simulations begin at 136 ka when the climate was substantially colder. As a result, the ice sheet model is initiated with an ice sheet in equilibrium with the 136 ka climate. The ice sheet model is spun-up for 50 000 yr in anomaly mode using the 136 ka climatology. This method requires GCM monthly mean changes in precipitation and near-surface temperature (defined relative to a pre-industrial climate) to be superimposed onto a present day reference climatology used by the surface mass balance model in Glimmer. Anomaly coupling is used to reduce climate model bias both for precipitation and temperature which affects the ice sheet model output, as in previous studies (Lunt et al., 2008, 2009).

In order to assess the sensitivity of ice sheet model results to the climate model used we compared offline forcing of the ice sheet model with two different 125 ka model climatologies (HadCM3 used here and the CCSM3 model). This comparison showed that, compared with the sensitivity to internal parameters (given in Table 1 and outlined in Stone et al., 2010), the GrIS evolution is insensitive to the climate model used.

Computationally, it is not yet feasible to run HadCM3 fully coupled (two-way) with Glimmer for the timescales of thousands of years, such as through the LIG. A methodology is developed based on that of Deconto and Pollard (2003) in order to account for a transient climate which evolves as the ice sheet volume evolves, whilst minimising computational expense. It takes into account a changing climate as a result of the change in ice sheet geometry by including the elevation-temperature feedback and an approximation to the albedo feedback. A total of 16 000 yr are modelled, representing the time period from 136 to 120 ka. Figure 4 shows a diagram of the coupling process, which is outlined in detail below. The monthly average climate, CL (t), is linearly interpolated along the time-axis from 136 to 130 ka where the notation $\mathrm{cl}_{\mathrm{year}}^{\text{state of Greenland}}$ is used (i.e. state of Greenland in HadCM3 is either ice covered: ice, partial ice: pice or ice-free: 0),

$$\mathrm{CL}\ (t) = \frac{\mathrm{cl}_{130}^{\mathrm{ice}} - \mathrm{cl}_{136}^{\mathrm{ice}}}{t_1} t + \mathrm{cl}_{136}^{\mathrm{ice}}. \tag{1}$$

The interpolation is between the 136 ka climate, $\mathrm{cl}_{136}^{\mathrm{ice}}$, and the 130 ka climate, $\mathrm{cl}_{130}^{\mathrm{ice}}$, where t_1 is 6000 model years. Glimmer is initiated with the equilibrated ice sheet geometry which was obtained by forcing Glimmer offline with the constant 136 ka climate. At 130 ka the climate is allowed to evolve each year between the three climate scenarios (with a GrIS, a partial GrIS and without a GrIS) according to a weighting function defined by the ratio of the ice volume (vol (t)) at time t and the ice volume predicted at 130 ka (vol (130)) by the ice sheet model. Between 130 and 125 ka the following linear interpolations are performed (represented by the solid blue, orange and red arrows respectively in Fig. 4) similar to Eq. (1)

$$\mathrm{cl}^{\mathrm{ice}}\ (t) = \frac{\mathrm{cl}_{125}^{\mathrm{ice}} - \mathrm{cl}_{130}^{\mathrm{ice}}}{t_2} t + \mathrm{cl}_{130}^{\mathrm{ice}}, \tag{2}$$

$$\mathrm{cl}^{\mathrm{pice}}\ (t) = \frac{\mathrm{cl}_{125}^{\mathrm{pice}} - \mathrm{cl}_{130}^{\mathrm{pice}}}{t_2} t + \mathrm{cl}_{130}^{\mathrm{pice}}, \tag{3}$$

and

$$\mathrm{cl}^{0}\ (t) = \frac{\mathrm{cl}_{125}^{0} - \mathrm{cl}_{130}^{0}}{t_2} t + \mathrm{cl}_{130}^{0}, \tag{4}$$

where $\mathrm{cl}_{125}^{\mathrm{ice}}$ is the 125 ka climate with the GrIS present, $\mathrm{cl}_{125}^{\mathrm{pice}}$ and $\mathrm{cl}_{130}^{\mathrm{pice}}$ are the 125 and 130 ka climates respectively with a partial GrIS, cl_{125}^{0} and cl_{130}^{0} are the 125 and 130 ka

CPD
8, 2731–2776, 2012

climates respectively with the GrIS removed and t_2 is 5000 yr. Likewise, similar linear interpolations are also performed from 125 to 120 ka.

If the ice volume, vol (t), is greater than the partial ice volume (defined as: $\mathrm{vol}_{\mathrm{pice}} = 0.46\mathrm{vol}_{\mathrm{ice}}(130)$), then the climate, CL (t), at each year is now also weighted either towards the climate with a partial GrIS, $\mathrm{cl}^{\mathrm{pice}}(t)$, or the GrIS climate, $\mathrm{cl}^{\mathrm{ice}}(t)$, according to

$$\mathrm{CL}\ (t) = \left(\frac{\mathrm{vol}\ (t) - \mathrm{vol}_{\mathrm{ice}}\ (130)}{\mathrm{vol}_{\mathrm{ice}}\ (130) - \mathrm{vol}_{\mathrm{pice}}\ (130)}\right)\left(\mathrm{cl}^{\mathrm{ice}}\ (t) - \mathrm{cl}^{\mathrm{pice}}\ (t)\right) + \mathrm{cl}^{\mathrm{ice}}\ (t). \tag{5}$$

Alternatively, if the ice volume is less than the partial ice volume then the climate, CL (t), at each year is weighted either towards the climate with no GrIS, $\mathrm{cl}^{0}(t)$, or the partial GrIS climate, $\mathrm{cl}^{\mathrm{pice}}(t)$, according to

$$\mathrm{CL}\ (t) = \frac{\mathrm{vol}\ (t)}{\mathrm{vol}\ (130)}\left(\mathrm{cl}^{\mathrm{pice}}\ (t) - \mathrm{cl}^{0}\ (t)\right) + \mathrm{cl}^{0}\ (t). \tag{6}$$

4 The modelled climate of the Last Interglaciation

The GCM simulated annual average global temperature anomaly at 130 ka is only 0.13 °C relative to pre-industrial, consistent with the small mean annual forcing associated with the orbital configuration for the LIG. However, the seasonal temperature anomaly is −1.6 °C and 2.0 °C in the Northern Hemisphere for winter/summer, respectively. Figure 5 shows a comparison of the LIG simulated Northern Hemisphere maximum summer warming with reconstructed terrestrial temperature anomalies derived from ice cores, pollen and macrofossils (Anderson et al., 2006; Kaspar et al., 2005). Overall, the agreement is very good (see also Table 3). However, during the summer months the maximum LIG average temperature anomaly over Greenland is 3.5 °C, cooler than values inferred (4 to 5 °C) from the temperature reconstruction over this region (Anderson et al., 2006). This implies that the GrIS during the LIG was likely smaller

CPD
8, 2731–2776, 2012

than today and represents a minimum temperature anomaly estimate. Simulated LIG warmth in Greenland is sustained under a 130 and 125 ka climate but with significant cooling by 120 ka consistent with the change in summer insolation distribution (see Fig. 2). These changes are amplified by sea-ice feedbacks discussed below. However, comparisons with proxy estimates of temperature at the location of the NGRIP ice core show a simulated summer temperature of 4.2 °C ± 1.1 °C, and an annual precipitation weighted temperature of 3.3 °C, lower than the 5 °C estimate obtained from the ice core oxygen isotope record (Andersen et al., 2004). Over much of the Greenland region predicted annual precipitation rate changes throughout the LIG are small.

Since the ice sheet climate coupling requires a set of GCM simulations where the GrIS is removed and replaced with bare soil we can assess the climate of the extreme scenario of an ice-free Greenland under LIG climate conditions. At the location of the NGRIP ice core, simulated maximum annual precipitation weighted temperature anomalies relative to pre-industrial are in excess of 20 °C and the average maximum summer Greenland anomaly ranges from 14 to 16 °C for the time period 125 to 130 ka. These values are clearly greater than the annual proxy paleo-data estimate of 5 °C (Anderson et al., 2006), which supports the ice core evidence that the GrIS did not completely disappear during the LIG (Andersen et al., 2004).

The increased insolation relative to pre-industrial during the early part of the LIG results in spring/summer melting of Arctic sea-ice with reduced concentrations compared with pre-industrial throughout the summer months. At 130 ka sea-ice concentration is reduced by up to 40 % compared with the pre-industrial in the central part of the Arctic Ocean, similar to results from Otto-Bliesner et al. (2006). This reduction of summer sea-ice around the margins of Greenland results in a positive sea-ice-albedo feedback and contributes to the observed warming in this region, particularly in the Labrador Sea. At 125 ka there is still a reduction in sea-ice in the Arctic compared with the pre-industrial but only up to 20 % over the majority of the region. By 120 ka the summer sea-ice concentration is similar if not greater than the pre-industrial with over 50 % sea-ice present again in the vicinity of the Labrador Sea. This increase in sea-ice is attributed to the cooler climate as a result of reduced summer insolation forcings toward the termination of the LIG. Although this reduction in average sea-ice over the Arctic Ocean implies a significant temperature difference relative to pre-industrial, the inter-annual variability over the averaging period of the simulations ranges from ~ 0 to $+1\,^{\circ}$C and, therefore, results in the regional temperature differences being statistically insignificant (see Fig. 5).

5 GrIS contribution to the Last Interglacial highstand

In order to estimate the contribution of the GrIS to LIG sea-level change we drive 500 realisations of an ice sheet model with the GCM-predicted evolving climate from 136 to 120 ka. Consequently, ice sheet geometry is predicted throughout the LIG and compared with reconstructed ice-surface extent data as implied from various ice cores on Greenland. The impact of ice sheet model parametric uncertainty (Stone et al., 2010) on the evolution of the GrIS through the LIG is used to derive a probability density function of the Greenland contribution to LIG sea-level rise contingent on our modelling choices. This also takes into account the mismatch between present day observed and modelled ice sheets, most likely due to missing higher order physical ice dynamics and the inclusion of a parameterised surface mass balance scheme.

Figure 6a shows the evolution of absolute ice volume throughout the 16 000 yr ice sheet simulations. All 500 ice sheet model simulations show contraction of the ice sheet in response to peak LIG warming. It is possible to reject a number of the GrIS LHS experiments using proxy paleo data from the LIG. It has been shown that at the Summit (Raynaud et al., 1997) and NGRIP (Andersen et al., 2004) ice cores on Greenland, ice very likely persisted throughout most of the LIG at these locations. The Dye-3, Camp Century and Renland ice cores are not, however, used to reject/accept simulations, as the evidence for the presence of ice there is more equivocal. In addition, simulations which make a negative contribution to sea-level change are also rejected. As a result a subset of 73 simulations are selected according to this evidence from the ice core

Discussion Paper | Discussion Paper | Discussion Paper | Discussion Paper |

CPD

8, 2731–2776, 2012

Greenland ice sheet Last Interglacial sea-level contribution

E. J. Stone et al.

data; that is simulations where ice is absent at the NGRIP and Summit ice cores are rejected. The selected simulations are shown in Fig. 6b, including a representation of their ability to reproduce the modern day GrIS according to a skill-score (for a given set of input parameters θ) given by

$$s(\theta) = -\frac{1}{2n}\sum_{i=1}^{n}\frac{(x_i - f_i(\theta))^2}{\sigma^2 + \tau^2}, \tag{7}$$

where n is the number of grid-points, x_i is observational ice thickness at each grid-point i, $f_i(\theta)$ is the experimental ice thickness at each grid-point for each ensemble member, σ is the ice thickness Root Mean Squared Error (RMSE) of the median parameter set experiment in terms of the LHS shown in Fig. 1 and τ^2 is the observational error variance at each grid-point. The observational error is assumed to be constant across all grid-points. This skill-score for modern ice thickness measures the spatial fit over the model domain assuming the differences between model and observation at each grid-point location are independent and normally distributed. We calculate the differences with respect to the digital elevation model derived by Bamber et al. (2001), interpolated to a 20 km resolution.

The ice sheet retreats in all selected cases compared with the pre-industrial, in response to the orbitally induced warming, with minimum ice sheet volume reached between 125 ka and 120.5 ka. All simulations show recovery towards the end of the LIG in response to the reduction in summer insolation. This is also shown by the average temperature anomaly over the Greenland region which peaks at around 2 to 5 °C for the selected members of the ensemble (see Fig. 7). Maximum GrIS contribution to LIG sea-level rise ranges between 0.4 and 3.8 m (Fig. 6c). None of the accepted simulations show an absence of ice in the vicinity of the Dye-3 ice core in accordance with some evidence that ice persisted through the LIG at this location (Andersen et al., 2004; Willerslev et al., 2007). However, there is large uncertainty in the dating of basal ice at this location (Willerslev et al., 2007) which is why it is not appropriate to use this data as a direct constraint on GrIS extent. Figure 8 shows the GrIS geometries

CPD
8, 2731–2776, 2012

for parameter sets resulting in the maximum, minimum and most likely (according to the skill-score) contribution to LIG sea-level change. Also shown is the respective ensemble member modern day GrIS geometry (Fig. 8d–f). The most likely extent of the GrIS shows retreat from the northern margins but ice is still present over Central and Southern Greenland (Fig. 8b). This contrasts with several previous studies (Cuffey and Marshall, 2000; Tarasov and Peltier, 2003; Lhomme et al., 2005; Otto-Bliesner et al., 2006) where ice sheet retreat is sensitive in the south but not the north. However, this sensitivity of the northern margin agrees with other recent GrIS simulations (Fyke et al., 2011; Greve et al., 2011; Born and Nisancioglu, 2011; Quiquet, 2012). An isolated cap remains in the vicinity of the Camp Century and Renland ice core locations for all simulations where ice also persists in the Summit region, in agreement with evidence suggesting ice also persisted here (Johnsen et al., 2001). The drawdown of the ice surface at the Summit core location in Fig. 8a, b is ~ 450 m and ~ 60 m, respectively, consistent with ice core data (Raynaud et al., 1997). In contrast, Fig. 8c shows little change from the modern day ice sheet extent with an increase of ~ 50 m at the location of Summit.

5.1 Probabilisitc assessment of GrIS contribution to the LIG highstand

It is possible to derive a probabilistic assessment of GrIS contribution to LIG sea-level rise by considering the LIG paleo-evidence of the GrIS geometry, uncertainty in ice sheet model parameterisation and the ability of the ice sheet model to reproduce the modern day ice sheet. In this section we outline our probabilistic method followed by an assessment of the likely contribution of the GrIS to LIG sea-level rise including a sensitivity analysis to the method used.

5.1.1 Probabilistic method

From Bayes' Theorem for a continuous distribution:

$$P\left[\theta|Y\right] \propto P\left[\theta\right] P\left[Y|\theta\right], \quad (8)$$

CPD
8, 2731–2776, 2012

the posterior probability distribution ($P[\theta|Y]$) is proportional to the prior probability distribution ($P[\theta]$) multiplied by the likelihood function ($P[Y|\theta]$). The likelihood function, $P[Y|\theta]$, is calculated for each member of the ensemble from the skill-score given in Eq. (7).

$$P\left[Y|\theta\right] = A \cdot e^{s(\theta)} \cdot l\left(\theta\right), \tag{9}$$

where A is a normalising constant such that the $\sum P\left[Y|\theta\right] = 1$ and the logistic function, $l(\theta)$ accounts for the uncertainty as to where the simulated ice sheet margin lies relative to the ice core locations at the resolution of the ice sheet model domain

$$l\left(\theta\right) = \frac{1}{2}\left[1 - \tanh\left(\frac{Y\left(\theta\right) - Y_{\max}}{2l_w}\right)\right]. \tag{10}$$

$Y(\theta)$ is the maximum sea-level change for each member of the ensemble, $Y_{\max}$ is the maximum contribution to LIG sea-level rise from the accepted simulations (in this case 3.8 m) and l_w is the logistic width.

The prior probability distribution, $P[\theta]$, weights each ensemble member according to its parameter set probability. The most basic is that each parameter is uniformly distributed such that each ensemble member is equally weighted. However, according to Stone et al. (2010) the parameter sets can reasonably be weighted as Gaussian 2-sigma ranges such that the extreme parameter choices are penalised. Hence, we model the prior probability distribution as a multivariate Gaussian distribution

$$P\left[\theta\right] = \frac{1}{(2\pi)^{\frac{5}{2}} \cdot 2 \cdot \prod_{j=1}^{5} \sigma_j} \times \exp\left\{-\frac{1}{2}\sum_{j=1}^{5}\left(\frac{\theta_j - \mu_j}{2\sigma_j}\right)^2\right\}, \tag{11}$$

where θ_j is the value of each parameter j, σ_j is the standard deviation for each parameter and μ_j is the mean for each parameter range (see Table 1). A comparison of the derived probability density function between Gaussian and uniform prior probability distributions indicates the choice of prior probability distribution does not have a notable affect on the outcome of the overall probability density function.

CPD
8, 2731–2776, 2012
Greenland ice sheet Last Interglacial sea-level contribution
E. J. Stone et al.

Subsequently, the posterior probability distribution of the ensemble and the associated maximum LIG sea-level contribution are used to construct a probability density function using a Kernel density estimator (Wand and Jones, 1995; Bowman and Azzalini, 1997). A probability density function is a function that describes the relative likelihood of a variable (in this case maximum sea-level change) to take on a particular given value. The probability for the variable to fall within a particular region is given by the integral of this variable's density over the region. This integral must add up to one. A Kernel estimator is a non-parametric way of estimating the probability density function of a particular variable and is closely related to a histogram. Unlike a histogram, a smooth Kernel function rather than a discrete box is used and each of these is centred directly over each model output in order to remove the dependence of end points of bins which occurs using a histogram method (Wand and Jones, 1995). In this way the Kernel estimator smoothes out the contribution of each observed data point over a local neighbourhood to that data point. The Kernel density estimator at any point Y, $\hat{g}(Y)$, is of the form

$$\hat{g}(Y) = \frac{1}{n}\sum_{i=1}^{n} K\left(\frac{Y - Y_i}{h}\right), \tag{12}$$

where n is the number of ensemble members, K is a function satisfying $\int K(Y)\mathrm{d}Y = 1$, the Kernel, whose variance is controlled by the parameter, h (usually known as the window width or smoothing parameter). K is chosen to be a unimodal probability density function that is symmetric about zero. In this case we implement a normal density function $\left(K(Y) = \frac{1}{\sqrt{2\pi}}e^{-\frac{1}{2}Y^2}\right)$.

The choice of h is important since structure in the data can be lost by over-smoothing. Scott (1992) shows that the reference rule bandwidth with a normal Kernel is

$$h = (4/3)^{1/5}\hat{\sigma}n^{-1/5} \approx 1.06\hat{\sigma}n^{-1/5}, \tag{13}$$

where $\hat{\sigma}$ is the sample standard deviation for maximum LIG sea level and n is the sample number. Alternatively, we can choose a Kernel width based on the modern ice

CPD
8, 2731–2776, 2012

sheet volume ensemble distribution. Figure 9 shows Kernel widths that result in the measured ice volume lying 1, 1.5 and 2 standard deviations away from the mean of the ensemble. In this way the smoothing parameter accounts for the additional uncertainty in the ice sheet model resulting in overestimation of the modern day GrIS volume (see Fig. 6a).

5.1.2 Results and sensitiviities

From the ensemble of 500 simulations we have derived a probabilistic assessment of the likely contribution from the GrIS to LIG sea-level change (Fig. 10) with the uncertainty in the ice model parameter distributions, modern day GrIS observations and the location of the paleo-data constraints taken into account. Although the maximum contribution from all the selected simulations is 3.8 m, Fig. 10a shows the most likely maximum GrIS contribution to LIG sea-level change is 1.5 m with a 90 % probability that the maximum contribution falls between 0.3 and 3.6 m. Figure 11 shows the predicted ice extent that results in a sea-level contribution of 1.5 m for the LIG (Fig. 11b) derived from this probability density function. This shows a similar pattern of retreat from the north and south-west as the ensemble member with the highest skill-score. We further show that the maximum contribution range varies from a maximum of 0.2 to 4.7 m to a minimum between 0.5 to 2.4 m depending on the parameters chosen in the formulation of the density function which takes into account ice sheet model uncertainty. There is a 90 % probability of the GrIS contribution exceeding 0.6 m during the LIG and a 67 % probability of exceeding 1.3 m. However, it is unlikely (< 33 % probability) the contribution exceeded 2.2 m and very unlikely (< 10 %) that it exceeded 3.2 m (Fig. 10b). Compared with estimates of the LIG sea-level highstand (Muhs et al., 2002; Rostami et al., 2000; Kopp et al., 2009) exceeding 4 m, we find that sources other than the GrIS are required to account for this high sea-level, such as the West Antarctic ice sheet (Scherer et al., 1998; Huybrechts, 2002) and/or the Canadian icefields (Otto-Bliesner et al., 2006).

In order to assess the sensitivity of our probability density function to various uncertainties in its construction we first examined the effect of varying the Kernel width. Figure 12 shows the case where the Kernel width is applied to the LIG for the optimal width (0.40 m according to Eq. 13), and the modern day observation lying one (h = 1.50 m) and two (h = 0.75 m) standard deviations away from the modern modelled ensemble mean. Although the peak of the probability density function does not change, the upper tail is sensitive to the Kernel width with a very likely sea-level contribution exceedance ranging between 3.1 and 4.1 m. The case with the optimal Kernel width assumes the anomaly in ice volume between the LIG and present day being biased in a consistent way. The alternative extreme scenario is the case where the uncertainty in the anomaly is equivalent to the model error such that the modern day ensemble lies only one standard deviation away from the observation (h = 1.50 m). We choose a Kernel width of half this width, 0.75 m, as our most plausible case, described above and shown in Fig. 10.

In order to further address the sensitivity of the probability density function to uncertainty we also varied σ (Fig. 13a), the observational error on modern day ice thickness (τ) (Fig. 13b) (both given as input in Eq. 7) and the width of the logistic function (Fig. 13c). Figure 13a shows when σ is equal to zero, the peak of the probability density function coincides closely with the simulation with the highest skill-score. The spread shown is a result of the Kernel smoothing method used. When all simulations have equal skill (no weighting) the probability density function shows a similar response to when σ is equal to the RMSE of the median experiment. The vertical accuracy of observational ice thickness is between 10 and 100 m (Bamber et al., 2001; Layberry and Bamber, 2001) while Bogorodskiy (1985) reports that a typical radar-sounding survey has an inherent uncertainty of about 15 m for ice depth measurements. Figure 13b shows that the observation error between 10 and 100 m makes no noticeable change to the overall probability density function. Therefore, we use a value of 15 m. Figure 13c shows that the choice of the logistic width parameter does show some sensitivity for the upper tail of the probability density function. In this case a value of 0.2 m is selected.

CPD
8, 2731–2776, 2012

We also performed an ensemble of simulations where only two modelled climates (with and without the GrIS) were used in the coupling method illustrated in Fig. 4. We found that although this increased the number of accepted simulations it did not result in a notable difference in the overall structure of the probabilistic distribution of GrIS contribution to LIG sea-level.

Finally, if the recent NEEM ice core drilling project reveals that ice persisted throughout the LIG at this location, then the GrIS contribution to LIG sea-level rise can be constrained further (61 accepted simulations compared with 73 when NEEM is not included) with values very likely (> 90 % probability) greater than 0.5 m but very unlikely (< 10 % probability) greater than 2.8 m (see Fig. 14).

6 Discussion and conclusions

There are several caveats that should be discussed in the context of this study. Firstly, the uncertainty in dating basal ice limits to an extent the usefulness of this binary criterion. With the advent of new improved ice cores in the future (such as NEEM) it may be possible to preferentially weight the skill toward these improved ice cores. In the future other aspects of the new ice-cores could also be used for model evaluation, e.g. downcore temperature profiles. However, uncertainties associated with these observations are currently quite large.

Secondly, these results, of course, are somewhat limited by the absence of climate model uncertainty. We use only one model where we linearly interpolate between three possible extreme LIG climate states. It is difficult to estimate the uncertainty in the LIG climate since there is only limited data for this time. Future work could assess the impact of structural climate model error on LIG sea-level change as part of the paleo model inter-comparison project 3 (PMIP3).

Thirdly, recent work (van de Berg et al., 2011; Robinson et al., 2011) has shown that temperature-melt relationships are dependent on insolation and as such the PDD method for predicting surface mass balance change during the LIG may not be suitable

CPD
8, 2731–2776, 2012

due to its different insolation forcing compared with today. However, although the mass balance scheme used in this study does not take into account directly the radiative forcing, it does indirectly because the GCM sees the full insolation change, which then modifies the seasonality of the surface temperature which drives the PDD scheme.

Fourthly, and perhaps most critically, the majority of the ensemble have an associated modern ice sheet which is too large (Fig. 6a, b), a feature of many ice sheet models (Ridley et al., 2005; Ritz et al., 1997; Robinson et al., 2011). This is partly due to additional ice at the margins not captured in the ice surface extent observation (Bamber et al., 2001) which includes only the contiguous ice sheet. In common with many other studies (Robinson et al., 2011; Lhomme et al., 2005), we assume that the predicted LIG volume anomaly with respect to the predicted modern is more robust. This is because the overestimation of volume, which is thought to result from the lack of higher-order terms in the ice-flow equations, is likely to affect both modern and LIG ice sheets in a consistent manner. In order, to account for potential bias, however, we choose a plausible probability density function that takes into account this uncertainty. The skill-score used to generate the probability density function (Eq. 7) does also ensure that the simulations which have the best representation of the modern ice sheet contribute most to the probability density function.

Our climate model, when forced with LIG insolation anomalies, shows good agreement with maximum summer warmth from LIG proxy temperature estimates in the Arctic region. We show that the GrIS contribution to LIG sea-level change, consistent with ice core data, is between 0.4 m and 3.8 m. However, it is very likely that the GrIS contributed between 0.3 and 3.6 m to LIG sea-level rise, lower than the range of previous recent estimates, of 2.7 to 4.5 m (Tarasov and Peltier, 2003; Robinson et al., 2011; Cuffey and Marshall, 2000). Our estimate is more reliable because it derives from a full probabilistic analysis, taking into account ice sheet model and data uncertainties. We also show that ice persists throughout the LIG at the Dye-3 ice core for all accepted simulations consistent with the suggestion that ice at the base of Dye-3 may predate

CPD
8, 2731–2776, 2012

the beginning of the LIG (Willerslev et al., 2007; Colville et al., 2011) although dating of basal ice at this location is equivocal (Willerslev et al., 2007).

In conclusion, this study emphasises the importance of including ice sheet model parametric uncertainty and paleo-data as well as modern observations, in the context of a probabilistic assessment when evaluating the impact of the Arctic on climate change.

Acknowledgements. This was work was carried out with funding from a NERC studentship and the European project Past4Future. This is Past4Future contribution no. 28. The research leading to these results has received funding from the European Union's Seventh Framework programme (FP7/2007–2013) under grant agreement no 243908, "Past4Future. Climate change – Learning from the past climate".

References

Andersen, K. K., Azuma, N., Barnola, J. M., Bigler, M., Biscaye, P., Caillon, N., Chappellaz, J., Clausen, H. B., DahlJensen, D., Fischer, H., Fluckiger, J., Fritzsche, D., Fujii, Y., Goto-Azuma, K., Gronvold, K., Gundestrup, N. S., Hansson, M., Huber, C., Hvidberg, C. S., Johnsen, S. J., Jonsell, U., Jouzel, J., Kipfstuhl, S., Landais, A., Leuenberger, M., Lorrain, R., Masson-Delmotte, V., Miller, H., Motoyama, H., Narita, H., Popp, T., Rasmussen, S. O., Raynaud, D., Rothlisberger, R., Ruth, U., Samyn, D., Schwander, J., Shoji, H., Siggard-Andersen, M. L., Steffensen, J. P., Stocker, T., Sveinbjornsdottir, A. E., Svensson, A., Takata, M., Tison, J. L., Thorsteinsson, T., Watanabe, O., Wilhelms, F., White, J. W. C., and NGRIP: High-resolution record of Northern Hemisphere climate extending into the last interglacial period, Nature, 431, 147–151, 2004.

Anderson, P., Bermike, O., Bigelow, N., Brigham-Grette, J., Duvall, M., Edwards, M., Frechette, B., Funder, S., Johnsen, S., Knies, J., Koerner, R., Lozhkin, A., Marshall, S., Matthiessen, J., Macdonald, G., Miller, G., Montoya, M., Muhs, D., Otto-Bliesner, B., Overpeck, J., Reeh, N., Sejrup, H. P., Spielhagen, R., Turner, C., Velichko, A., and Members, C.-L. I. P.: Last Interglacial Arctic warmth confirms polar amplification of climate change, Quaternary Sci. Rev., 25, 1383–1400, 2006.

Bamber, J. L., Layberry, R. L., and Gogineni, P.: A new ice thickness and bed data set for the Greenland ice sheet, 1. Measurement, data reduction, and errors, J. Geophys. Res., 106, 33773–33780, 2001.

Berger, A. and Loutre, M. F.: Insolation values for the climate of the last 10 million years, Quaternary Sci. Rev., 10, 297–317, 1991.

Bogorodskiy, V. V.: Radioglaciology, D. Reidel Publishing Company, Dordrecht, 1985.

Born, A. and Nisancioglu, K. H.: Melting of Northern Greenland during the last interglacial, The Cryosphere Discuss., 5, 3517–3539, doi:10.5194/tcd-5-3517-2011, 2011.

Bowman, A. W. and Azzalini, A.: Applied smoothing techniques for data analysis: the kernel approach with s-plus illustrations, Vol. 18, Oxford Univ. Press, New York, 1997.

Cattle, H. and Crossley, J.: Modeling arctic climate-change, Philos. T. Roy. Soc. Lond. A, 352, 201–213, 1995.

Colville, E. J., Carlson, A. E., Beard, B. L., Hatfield, R. G., Stoner, J. S., Reyes, A. V., and Ullman, D. J.: Sr-Nd-Pb isotope evidence for ice-sheet presence on Southern Greenland during the last interglacial, Science, 333, 620–623, doi:10.1126/science.1204673, 2011.

Cox, P. M., Betts, R. A., Bunton, C. B., Essery, R. L. H., Rowntree, P. R., and Smith, J.: The impact of new land surface physics on the GCM simulation of climate and climate sensitivity, Clim. Dynam., 15, 183–203, 1999.

Cuffey, K. M. and Marshall, S. J.: Substantial contribution to sea-level rise during the last interglacial from the Greenland ice sheet, Nature, 404, 591–594, 2000.

DeConto, R. M. and Pollard, D.: Rapid Cenozoic glaciation of Antarctica induced by declining atmospheric CO_2, Nature, 421, 245–249, 2003.

Edwards, J. M. and Slingo, A.: Studies with a flexible new radiation code. 1. Choosing a configuration for a large-scale model, Q. J. Roy. Meteor. Soc., 122, 689–719, 1996.

Fyke, J. G., Weaver, A. J., Pollard, D., Eby, M., Carter, L., and Mackintosh, A.: A new coupled ice sheet/climate model: description and sensitivity to model physics under Eemian, Last Glacial Maximum, late Holocene and modern climate conditions, Geosci. Model Dev., 4, 117–136, doi:10.5194/gmd-4-117-2011, 2011.

Gent, P. R. and McWilliams, J. C.: Isopycnal mixing in ocean circulation models, J. Phys. Oceanogr., 20, 150–155, 1990.

Gordon, C., Cooper, C., Senior, C. A., Banks, H., Gregory, J. M., Johns, T. C., Mitchell, J. F. B., and Wood, R. A.: The simulation of SST, sea ice extents and ocean heat transports in a ver-

CPD
8, 2731–2776, 2012
Greenland ice sheet Last Interglacial sea-level contribution
E. J. Stone et al.

sion of the Hadley Centre coupled model without flux adjustments, Clim. Dynam., 16, 147–168, 2000.
Gregory, D. and Rowntree, P. R.: A mass flux convection scheme with representation of cloud ensemble characteristics and stability-dependent closure, Mon. Weather Rev., 118, 1483–1506, 1990.
Gregory, D., Kershaw, R., and Inness, P. M.: Parametrization of momentum transport by convection. II: Tests in single-column and general circulation models, Q. J. Roy. Meteor. Soc., 123, 1153–1183, 1997.
Gregory, D., Shutts, G. J., and Mitchell, J. R.: A new gravity-wave-drag scheme incorporating anisotropic orography and low-level wave breaking: impact upon the climate of the UK Meteorological Office Unified Model, Q. J. Roy. Meteor. Soc., 124, 463–493, 1998.
Gregory, J. M. and Mitchell, J. F. B.: The climate response to CO_2 of the Hadley Centre coupled AOGCM with and without flux adjustment, Geophys. Res. Lett., 24, 1943–1946, 1997.
Greve, R.: Relation of measured basal temperatures and the spatial distribution of the geothermal heat flux for the Greenland ice sheet, Ann. Glaciol., 42, 424–432, 2005.
Greve, R., Saito, F., and Abe-Ouchi, A.: Initial results of the SeaRISE numerical experiments with the models SICOPOLIS and IcIES for the Greenland ice sheet, Ann. Glaciol., 52, 23–30, 2011.
Hanna, E., Huybrechts, P., Janssens, I., Cappelen, J., Steffen, K., and Stephens, A.: Runoff and mass balance of the Greenland ice sheet: 1958–2003, J. Geophys. Res., 110, D13108, doi:10.1029/2004JD005641, 2005.
Hibler, W. D.: A dynamic thermodynamic sea ice model, J. Phys. Oceanogr., 9, 815–846, 1979.
Huybrechts, P.: Sea-level changes at the LGM from ice-dynamic reconstructions of the Greenland and Antarctic ice sheets during the glacial cycles, Quaternary Sci. Rev., 21, 203–231, 2002.
Johnsen, S. J., DahlJensen, D., Gundestrup, N., Steffensen, J. P., Clausen, H. B., Miller, H., Masson-Delmotte, V., Sveinbjornsdottir, A. E., and White, J.: Oxygen isotope and palaeotemperature records from six Greenland ice-core stations: Camp Century, Dye-3, GRIP, GISP2, Renland and NorthGRIP, J. Quaternary Sci., 16, 299–307, 2001.
Junge, M. M., Blender, R., Fraedrich, K., Gayler, V., Luksch, U., and Lunkeit, F.: A world without Greenland: impacts on the Northern Hemisphere winter circulation in low- and high-resolution models, Clim. Dynam., 24, 297–307, doi:10.1007/s00382-004-0501-2, 2005.

CPD
8, 2731–2776, 2012

Kaspar, F., Kuhl, N., Cubasch, U., and Litt, T.: A model-data comparison of European temperatures in the Eemian interglacial, Geophys. Res. Lett., 32, L11703, doi:10.1029/2005GL022456, 2005.
Kienast, F., Tarasov, P., Schirrmeister, L., Grosse, G., and Andreev, A. A.: Continental climate in the East Siberian Arctic during the last interglacial: implications from palaeobotanical records, Global Planet. Change, 60, 535–562, 2008.
Kopp, R. E., Simons, F. J., Mitrovica, J. X., Maloof, A. C., and Oppenheimer, M.: Probabilistic assessment of sea level during the last interglacial stage, Nature, 462, 863–868, 2009.
Lambeck, K. and Nakiboglu, S. M.: Seamount loading and stress in the ocean lithosphere, J. Geophys. Res., 85, 6403–6418, 1980.
Laskar, J., Robutel, P., Joutel, F., Gastineau, M., Correia, A. C. M., and Levrard, B.: A long-term numerical solution for the insolation quantities of the Earth, Astron. Astrophys., 428, 261–285, 2004.
Layberry, R. L. and Bamber, J. L.: A new ice thickness and bed data set for the Greenland ice sheet 2. Relationship between dynamics and basal topography, J. Geophys. Res., 106, 33781–33788, 2001.
Letréguilly, A., Reeh, N., and Huybrechts, P.: The Greenland ice sheet through the last glacial-interglacial cycle, Global Planet. Change, 90, 385–394, 1991.
Lhomme, N., Clarke, G. K. C., and Marshall, S. J.: Tracer transport in the Greenland ice sheet: constraints on ice cores and glacial history, Quaternary Sci. Rev., 24, 173–194, 2005.
Loulergue, L., Parrenin, F., Blunier, T., Barnola, J.-M., Spahni, R., Schilt, A., Raisbeck, G., and Chappellaz, J.: New constraints on the gas age-ice age difference along the EPICA ice cores, 0–50 kyr, Clim. Past, 3, 527–540, doi:10.5194/cp-3-527-2007, 2007.
Loutre, M. F., Berger, A., Crucifix, M., Desprat, S., and Sánchez-Gõni, M. F.: Interglacials as simulated by the LLN 2-D NH and MoBidiC climate models, in: The Climate of Past Interglacials, Vol. 7, 1st Edn., edited by: Sirocko, F., Claussen, M., Litt, T., and Sánchez-Gõni, M. F., Development in Quaternary Science, 7, Elsevier, Oxford, 547–561, 2007.
Lunt, D. J., Foster, G. L., Haywood, A. M., and Stone, E. J.: Late Pliocene Greenland glaciation controlled by a decline in atmospheric CO_2 levels, Nature, 454, 1102–1105, 2008.
Lunt, D. J., Haywood, A. M., Foster, G. L., and Stone, E. J.: The Arctic cryosphere in the Mid-Pliocene and the future, Philos. T. Roy. Soc. Lond. A, 367, 49–67, 2009.
Luthi, D., Le Floch, M., Bereiter, B., Blunier, T., Barnola, J. M., Siegenthaler, U., Raynaud, D., Jouzel, J., Fischer, H., Kawamura, K., and Stocker, T. F.: High-resolution car-

Discussion Paper | Discussion Paper | Discussion Paper | Discussion Paper |

CPD
8, 2731–2776, 2012

Greenland ice sheet Last Interglacial sea-level contribution

E. J. Stone et al.

bon dioxide concentration record 650 000–800 000 yr before present, Nature, 453, 379–382, doi:10.1038/Nature06949, 2008.
Milankovitch, M.: Kanon der Erdbestrahlungen und seine Anwendung auf das Eiszeitenproblem Belgrade, (English translation Canon of Insolation and the Ice-Age Problem), Israel Program for Scientific Translations, 1969, Jerusalem, 1941.
Milton, S. F. and Wilson, C. A.: The impact of parameterized subgrid-scale orographic forcing on systematic errors in a global NWP model, Mon. Weather Rev., 124, 2023–2045, 1996.
Montoya, M., von Storch, H., and Crowley, T. J.: Climate simulation for 125 kyr BP with a coupled ocean-atmosphere general circulation model, J. Climate, 13, 1057–1072, 2000.
Muhs, D. R., Ager, T. A., and Begét, J. E.: Vegetation and paleoclimate of the last interglacial period, Central Alaska, Quaternary Sci. Rev., 20, 41–61, 2001.
Muhs, D. R., Simmons, K. R., and Steinke, B.: Timing and warmth of the last interglacial period: new U-series evidence from Hawaii and Bermuda and a new fossil compilation for North America, Quaternary Sci. Rev., 21, 1355–1383, 2002.
Otto-Bliesner, B. L., Marsha, S. J., Overpeck, J. T., Miller, G. H., Hu, A. X., and CAPE: Simulating Arctic climate warmth and icefield retreat in the last interglaciation, Science, 311, 1751–1753, 2006.
Payne, A. J.: A thermomechanical model of ice flow in West Antarctica, Clim. Dynam., 15, 115–125, 1999.
Pépin, L., Raynaud, D., Barnola, J. M., and Loutre, M. F.: Hemispheric roles of climate forcings during glacial-interglacial transitions as deduced from the Vostok record and LLN-2D model experiments, J. Geophys. Res., 106, 31885–31892, 2001.
Petersen, G. N., Kristjánsoon, J. E., and Ólafsson, H.: Numerical simulations of Greenland's impact on the Northern Hemisphere winter circulation, Tellus, 56, 102–111, 2004.
Petit, J. R., Jouzel, J., Raynaud, D., Barkov, N. I., Barnola, J. M., Basile, I., Bender, M., Chappellaz, J., Davis, M., Delaygue, G., Delmotte, M., Kotlyakov, V. M., Legrand, M., Lipenkov, V. Y., Lorius, C., Pepin, L., Ritz, C., Saltzman, E., and Stievenard, M.: Climate and atmospheric history of the past 420 000 yr from the Vostok ice core, Antarctica, Nature, 399, 429–436, 1999.
Pollard, D. and Thompson, S. L.: Driving a high-resolution dynamic ice sheet model with GCM climate: ice-sheet initiation at 116 000 BP, Ann. Glaciol., 25, 296–304, 1997.

Pope, V. D., Gallani, M. L., Rowntree, P. R., and Stratton, R. A.: The impact of new physical parametrizations in the Hadley Centre climate model: HadAM3, Clim. Dynam., 16, 123–146, 2000.
Quiquet, A.: Reconstruction de la calotte glaciaire du Groenland au cours du dernier cycle glaciaire-interglaciaire, P.h.D, Labortoire de Glaciologie et de Géophysique de l'Environment, Université de Grenoble, 1–167, 2012.
Raynaud, D., Chappellaz, J., Ritz, C., and Martinerie, P.: Air content along the Greenland ice core project core: a record of surface climatic parameters and elevation in Central Greenland, J. Geophys. Res., 102, 26607–26613, 1997.
Reeh, N.: Paramterization of melt rate and surface temperature on the Greenland ice sheet, Polarforschung, 59, 113–128, 1991.
Ridley, J. K., Huybrechts, P., Gregory, J. M., and Lowe, J. A.: Elimination of the Greenland ice sheet in a high CO_2 climate, J. Climate, 18, 3409–3427, 2005.
Ritz, C., Fabre, A., and Letréguilly, A.: Sensitivity of a Greenland ice sheet model to ice flow and ablation parameters: consequences for the evolution through the last climatic cycle, Clim. Dynam., 13, 11–24, 1997.
Robinson, A., Calov, R., and Ganopolski, A.: Greenland ice sheet model parameters constrained using simulations of the Eemian Interglacial, Clim. Past, 7, 381–396, doi:10.5194/cp-7-381-2011, 2011.
Rostami, K., Peltier, W. R., and Mangini, A.: Quaternary marine terraces, sea-level changes and uplift history of Patagonia, Argentina: comparisons with predictions of the ICE-4G (VM2) model of the global process of glacial isostatic adjustment, Quaternary Sci. Rev., 19, 1495–1525, 2000.
Rutt, I. C., Hagdorn, M., Hulton, N. R. J., and Payne, A. J.: The glimmer community ice sheet model, J. Geophys. Res., 114, F02004, doi:10.1029/2008JF001015, 2009.
Scherer, R. P., Aldahan, A., Tulaczyk, S., Possnert, G., Engelhardt, H., and Kamb, B.: Pleistocene collapse of the West Antarctic ice sheet, Science, 281, 82–85, 1998.
Scott, C.: Multivariate Density Estimation: Theory, Practice and Visualization, John Wiley & Sons, New York, 1992.
Siddall, M., Chappell, J., and Potter, E.-K.: Eustatic sea level during past interglacials, in: The Climate of Past Interglacials, Vol. 7, 1st Edn., edited by: Sirocko, F., Claussen, M., Litt, T., and Sánchez-Gõni, M. F., Development in Quaternary Science, 7, Elsevier, Oxford, 75–92, 2007.

Slowey, N. C., Henderson, G. M., and Curry, W. B.: Direct U-Th dating of marine sediments from the two most recent interglacial periods, Nature, 383, 242–244, 1996.
Stone, E. J., Lunt, D. J., Rutt, I. C., and Hanna, E.: Investigating the sensitivity of numerical model simulations of the modern state of the Greenland ice-sheet and its future response to climate change, The Cryosphere, 4, 397–417, doi:10.5194/tc-4-397-2010, 2010.
Tarasov, L. and Peltier, W. R.: Greenland glacial history, borehole constraints, and Eemian extent, J. Geophys. Res., 108, 2143, doi:10.1029/2001JB001731, 2003.
Uppala, S. M., Kallberg, P. W., Simmons, A. J., Andrae, U., Da Costa Bechtold, V., Fiorino, M., Gibson, K., Haseler, J., Hernandez, A., Kelly, G. A., Li, X., Onogi, K., Saarinen, S., Sokka, N., Allan, R. P., Andersson, E., Arpe, K., Balmaseda, M. A., Beljaars, A. C., Van de Berg, L., Bidlot, J., Bormann, N., Caires, S., Chevallier, F., Dethof, A., Dragosavac, M., Fisher, M., Fuentes, M., Hagemann, S., Holm, E., Hoskins, B. J., Isaksen, L., Janssen, P. A. E. M., Jenne, R., Mcnally, A. P., Mahfouf, J.-F., Morcrette, J.-J., Rayner, N. A., Saunders, R. W., Simon, P., Sterl, A., Trenberth, K. E., Untch, A., Vasiljevic, D., Viterbo, P., and Woollen, J.: The ERA-40 re-analysis, Q. J. Roy. Meteor. Soc., 131, 2961–3013, 2005.
van de Berg, W. J., van den Broeke, M., Ettema, J., van Meijgaard, E., and Kaspar, F.: Significant contribution of insolation to Eemian melting of the Greenland ice sheet, Nat. Geosci., 4, 679–683, doi:10.1038/Ngeo1245, 2011.
Vizcaíno, M., Milkolajewicz, U., Groger, M., Maier-reimer, E., Schurgers, G., and Winguth, A. M. E.: Long-term ice sheet-climate interactions under anthropogenic greenhouse forcing simulated with a complex Earth system model, Clim. Dynam., 31, 665–690, doi:10.1007/s00382-008-0369-7, 2008.
Wand, M. P. and Jones, M. C.: Kernel Smoothing, 60, Chapman & Hall/CRC, Boca Raton, 1995.
Willerslev, E., Cappellini, E., Boomsma, W., Nielsen, R., Hebsgaard, M. B., Brand, T. B., Hofreiter, M., Bunce, M., Poinar, H. N., Dahl-Jensen, D., Johnsen, S., Steffensen, J. P., Bennike, O., Schwenninger, J. L., Nathan, R., Armitage, S., de Hoog, C. J., Alfimov, V., Christl, M., Beer, J., Muscheler, R., Barker, J., Sharp, M., Penkman, K. E. H., Haile, J., Taberlet, P., Gilbert, M. T. P., Casoli, A., Campani, E., and Collins, M. J.: Ancient biomolecules from deep ice cores reveal a forested Southern Greenland, Science, 317, 111–114, 2007.
Yin, Q. Z. and Berger, A.: Individual contribution of insolation and CO_2 to the interglacial climates of the past 800 000 yr, Clim. Dynam., 38, 709–724, 2012.

Table 1. List of five parameters varied according to ranges determined in the literature (Stone et al., 2010). Also included are the mean and standard deviation for each parameter used in Eq. (11).

Parameter	Range	Mean (μ)	Standard deviation (σ)
Positive degree day factor for snow, α_s (mm d^{-1} °C^{-1})	3.0 to 5.0	4.0	±1.2
Positive degree day factor for ice, α_i (mm d^{-1} °C^{-1})	8.0 to 20.0	14.0	±6.9
Enhancement flow factor, f	1.0 to 5.0	3.0	±2.3
Geothermal heat flux, G (mW m^{-2})	−61.0 to −38.0	−49.5	±13.3
Near surface lapse rate, L_G (°C km^{-1})	−8.2 to −4.0	−6.1	±2.4

CPD
8, 2731–2776, 2012

Table 2. The orbital parameters (from Milankovitch theory) for four time snapshots between 140 and 120 ka (Berger and Loutre, 1991). Also shown for comparison are the parameters for pre-industrial.

Time (ka)	Obliquity (°)	Eccentricity	Perihelion (day of year)
136	23.97	0.0367	35.1
130	24.25	0.0401	121.8
125	23.82	0.0423	200.0
120	23.04	0.0436	287.6
0	23.45	0.0172	2.6

CPD
8, 2731–2776, 2012

Table 3. Comparison of LIG temperature anomalies (in °C) derived from paleo-proxy reconstructions (Anderson et al., 2006) with the simulated maximum LIG summer temperature anomalies from HadCM3. All locations described are shown on Fig. 5. The values in brackets for comparison with ice core data on Greenland (NGRIP & Renland) refer to the warmest annual precipitation-weighted temperatures.

Location		Observed ΔT	Modeled ΔT
Greenland	Central Greenland, NGRIP (75.1° N, 42.3° W)	5	4.2 ± 1.1 (3.3)
	E Greenland, Renland (71.3° N, 26.7° W)	5	4.3 ± 1.9 (4.9)
	E Greenland, Jamesonland (72.0° N, 23.0° W)	5	2.2 ± 1.4
	NW Greenland,Thule (76.0° N, 68.0° W)	4	3.5 ± 1.4
Canada	Robinson Lake, Baffin Is. (63.0° N, 64.0° W)	5	1.4 ± 1.4
	Brother of Fog Lake, Baffin Is. (67.0° N, 63.0° W)	4	1.9 ± 1.6
	Fog Lake, N. Baffin Is. (67.2° N, 63.3° W)	3–4	1.9 ± 1.6
	Flitaway Beds, Baffin Is. (70.0° N, 75.0° W)	4–5	5.1 ± 1.0
	Amarok Lake, Baffin Is. (66.3° N, 65.8° W)	5–6	3.4 ± 1.2
Russia	NE Siberia (Chakota region) (68.0° N, 177.0° E)	4–8	2.6 ± 1.5
	Siberia (73.3° N, 141.5° E)	4–5	1.7 ± 1.5
	European Russia (White Sea) (63.0° N, 35.0° E)	4	3.6 ± 1.5
Alaska	Interior Alaska, Eva Creek (64.9° N, 147.9° W)	0–2	2.8 ± 1.6
	NW Alaska, Squirrel Lake (67.4° N, 160.7° W)	1–2	1.9 ± 1.7
	NW Alaska, Ahaliorak Lake (68.0° N, 153.0° W)	1–2	2.7 ± 1.7
	NW Alaska, Noatak Valley (68° N, 160° W)	0–2	1.9 ± 1.7
	North Coast Alaska (70.0° N, 150.0° W)	3	3.6 ± 1.9
Norway	60.2° N, 5° E	2.9	1.3 ± 1.2
Svalbard	78° N, 22° E	2–2.5	1.2 ± 1.5
North Atlantic	JPC8 (61° N, 28° W)	3–4	1.4 ± 0.8
	NA87-25 (55.2° N, 14.7° W)	1–2	0.9 ± 1.3
	CH69-K9 (41° N, 47° W)	−1	1.9 ± 1.3
	SU90-03 (40.5° N, 32.1° W)	0 ± 1	1.8 ± 1.1

CPD
8, 2731–2776, 2012

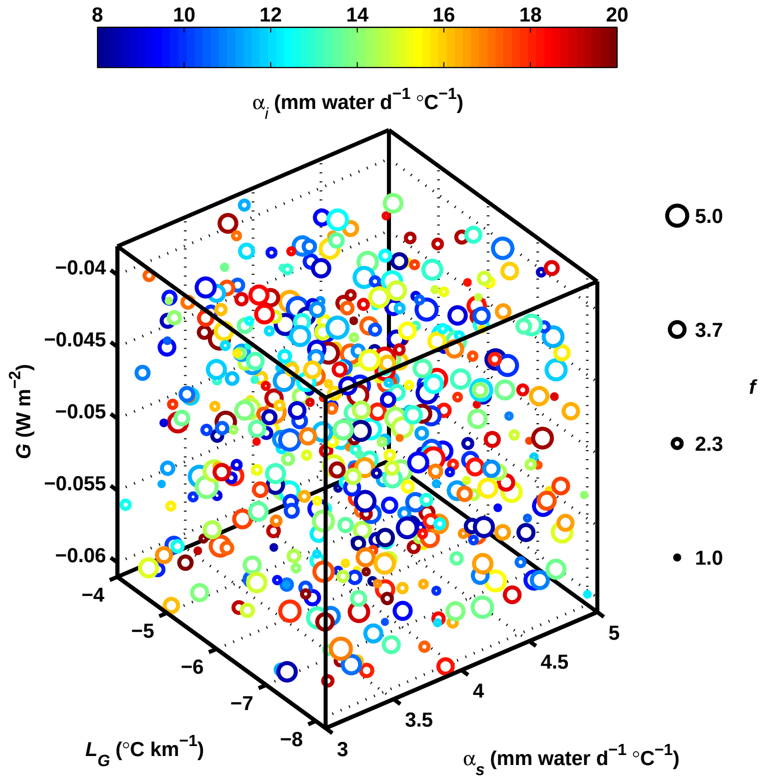

Fig. 1. Distribution of 500 experiments produced by Latin-Hypercube Sampling. In three dimensions geothermal heat flux (G), Positive Degree Day (PDD) factor for snow (α_s) and atmospheric vertical lapse rate (L_G) are shown. In addition, for each experiment the PDD factor for ice (α_i) is shown in terms of the colour-scale and the enhancement flow factor (f) in terms of the size of circle.

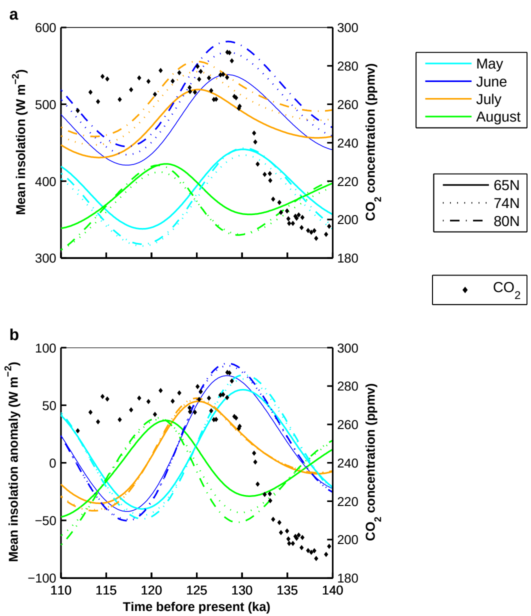

Fig. 2. Time series of LIG **(a)** insolation and **(b)** insolation anomaly relative to pre-industrial over Greenland for the period 140 to 110 ka. Insolation values are calculated using the numerical solution of Laskar et al. (2004). Also overlain is CO_2 concentration (ppmv) from the composite record of Luthi et al. (2008) based on data from Petit et al. (1999) and Pépin et al. (2001) for the LIG (they are on the EDC3 gas age scale, Loulergue et al., 2007). The colours correspond to the following months: May (light blue), June (blue), July (orange) and August (green). Line styles refer to different latitudes over Greenland.

CPD
8, 2731–2776, 2012

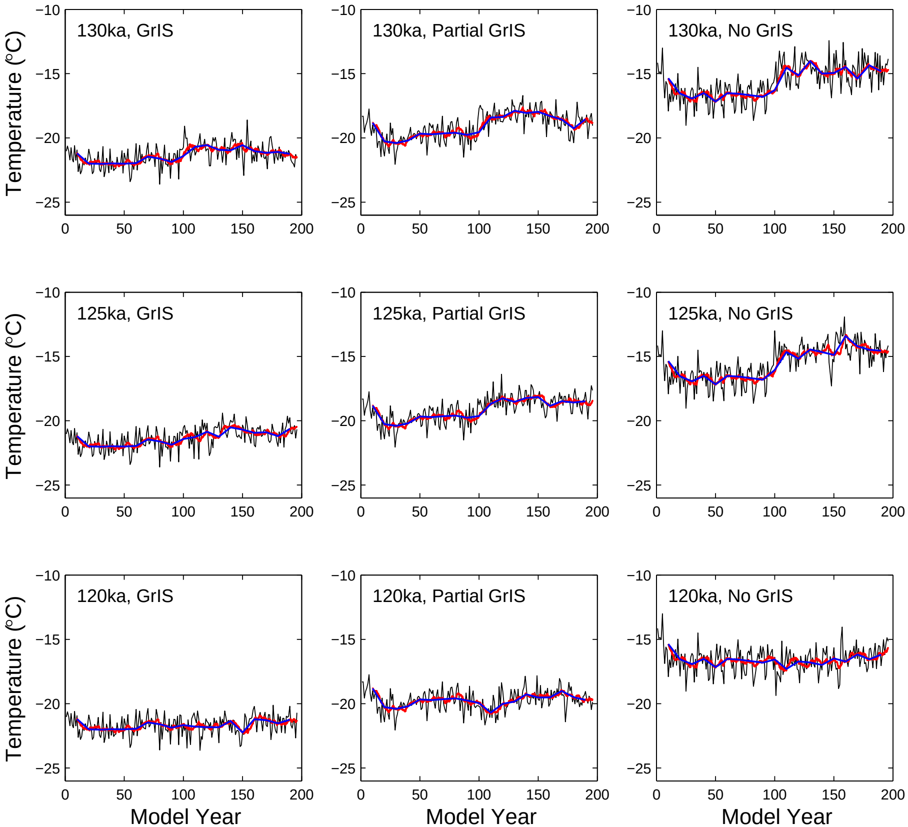

Fig. 3. Near-surface temperature time-series for the three LIG snapshots with a GrIS, partial GrIS and without a GrIS included. The first 100 yr represent pre-industrial greenhouse and orbital conditions. The last 100 yr are the temperature response to changed orbital parameters. The black line is the annual mean, red line is the 10 yr running average and the blue line is the 10 yr mean.

CPD
8, 2731–2776, 2012

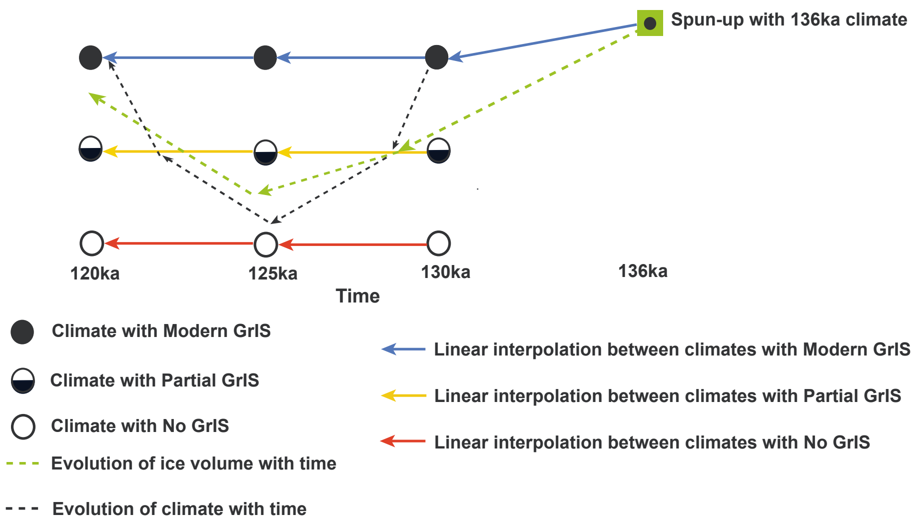

Fig. 4. Illustration of the coupling methodology between climate and ice sheet for the LIG. Simulations are run for a total of 16 000 model years, initiated with a climate representative of 136 ka (GrIS included). The transient climate evolves simultaneously with the ice sheet model. The climate is linearly interpolated from 136 to 130 ka. From 130 ka to 120 ka the climate evolves (black dashed arrow shows an example) according to a weighting towards either a transient climate where there is a modern day GrIS (black filled circles), one where there is a partial GrIS (black half filled circles) and where the GrIS is removed (black open circles). The weighting is based on the ratio of the previous years' ice volume relative to the ice volume at 130 ka. The green dashed arrow shows schematically the evolution of the ice sheet volume. See text for more details and equations.

CPD
8, 2731–2776, 2012

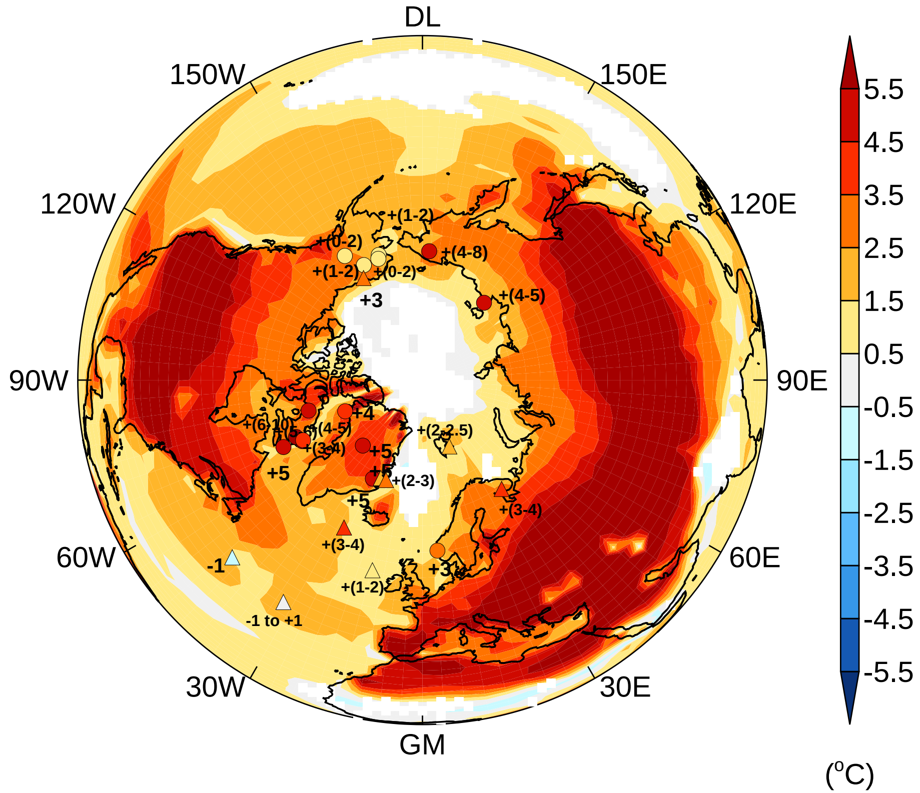

Fig. 5. Simulated maximum LIG Arctic summer (June, July, August) temperature anomaly relative to pre-industrial. Overlain is the maximum observed LIG summer temperature anomalies from paleo temperature proxies (terrestrial: circles and marine: triangles) (Anderson et al., 2006; Kaspar et al., 2005). White regions are not statistically significant (at the 95 % confidence interval).

CPD
8, 2731–2776, 2012

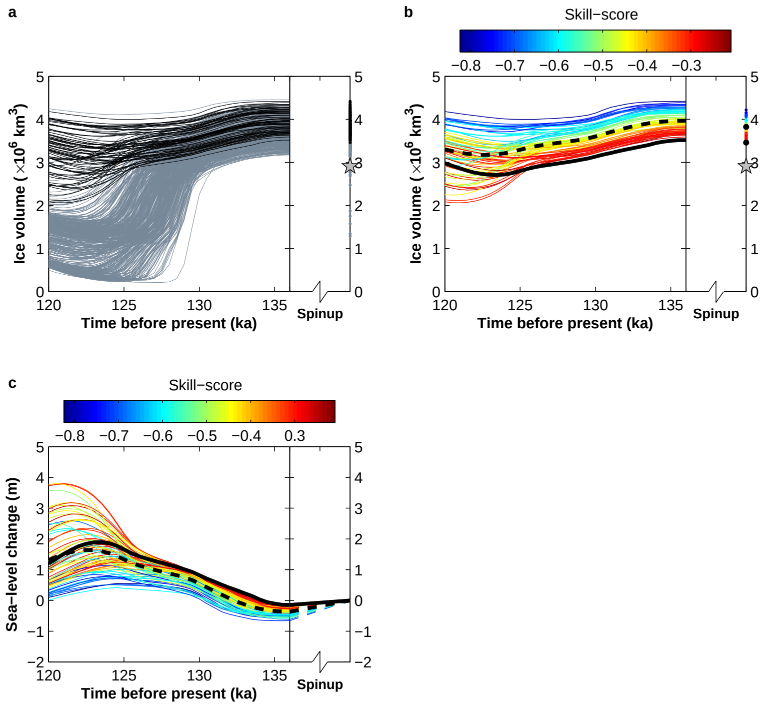

Fig. 6. Simulated LIG GrIS evolution from the ensemble of simulations. **(a)** GrIS volume evolution for all 500 configurations. Black lines show experiments where ice persisted at NGRIP and Summit. **(b)** Ice volume change for 73 selected simulations according to constraints at the Summit and NGRIP cores. **(c)** Change in GrIS sea-level contribution relative to present day for the selected simulations. Also shown on **(b)** is the skill-score for the simulated modern day GrIS (see Eq. 7) on the right-hand axis. The star represents the modern day observed GrIS volume (Bamber et al., 2001). The solid black line represents the simulation with the highest skill-score for the modern day GrIS. The dashed black line represents the average for all accepted simulations.

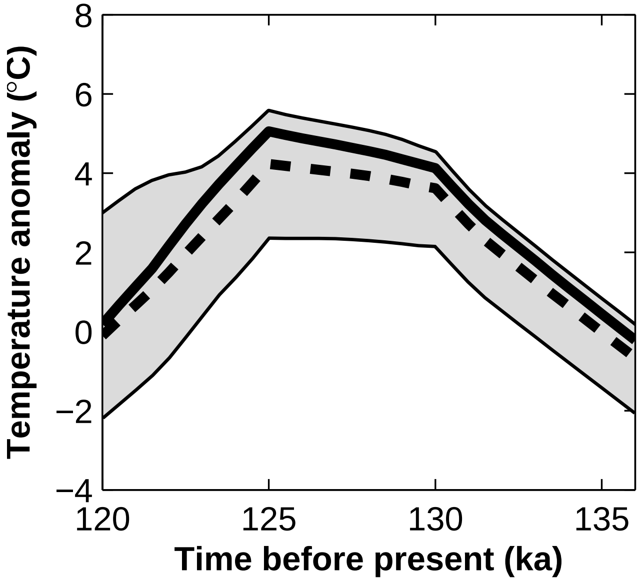

Fig. 7. LIG surface temperature anomaly (relative to pre-industrial) evolution, averaged over the Glimmer model domain for the valid simulations. Included is the change in temperature due to a lapse rate correction as a result of changing elevation as the ice sheet changes in response to the climate forcing. The solid back line represents the accepted simulation with the highest skill-score for the modern day GrIS. The dashed back line represents the average for all accepted simulations.

CPD
8, 2731–2776, 2012

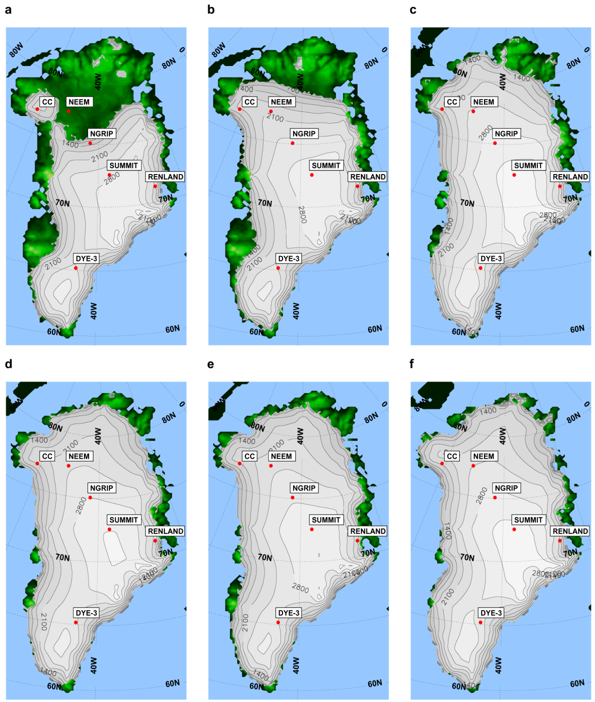

Fig. 8. Simulated range from the selected experiments for the minimum GrIS geometry during the LIG **(a–c)** and their respective modern day GrIS geometries **(d–f)**. **(a)** Extent of the GrIS for the maximum contribution (at 121.0 ka) to LIG sea-level change (+3.8 m), **(b)** the extent of the most likely contribution (at 123.5 ka) to LIG sea-level change (+1.5 m) and **(c)** the extent of the minimum contribution (at 125 ka) to LIG sea-level change (+0.4 m). Red spots show Greenland ice-core locations.

CPD
8, 2731–2776, 2012

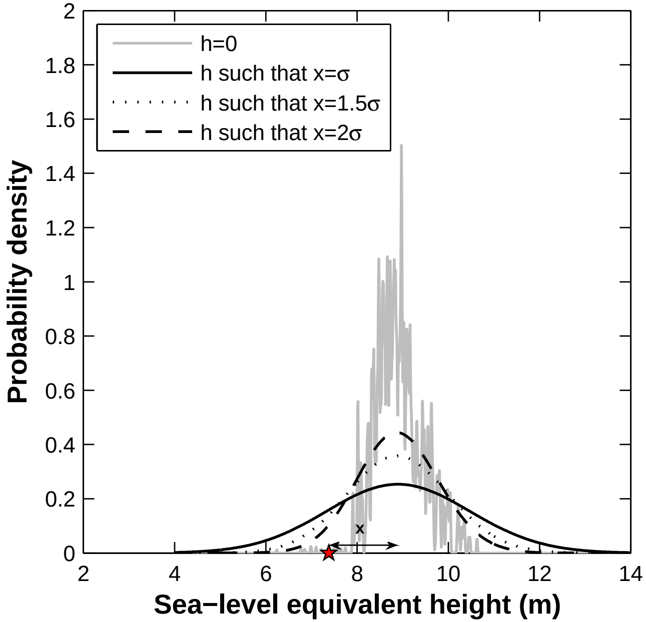

Fig. 9. Probability density functions constructed from the 500 member ensemble of modern day GrIS sea-level equivalent height. The red star denotes the observation from Bamber et al. (2001). The distance x represents the difference between the mean of the ensemble and the observation. The grey line shows the probability density function with no smoothing. The black lines show the cases where the smoothing parameter, h, results in a probability density function where $x = \sigma$ (dashed), $x = 1.5\sigma$ (dotted) and $x = 2\sigma$ (solid).

CPD
8, 2731–2776, 2012

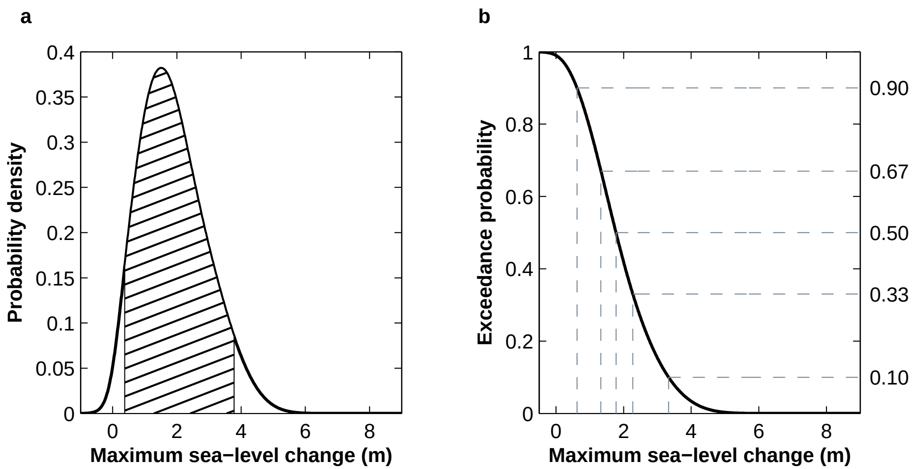

Fig. 10. GrIS maximum contribution to sea-level change during the LIG. **(a)** Probability density plot. The hashed region denotes the 90 % confidence interval (0.3 to 3.6 m). **(b)** Exceedance values for the probability distribution.

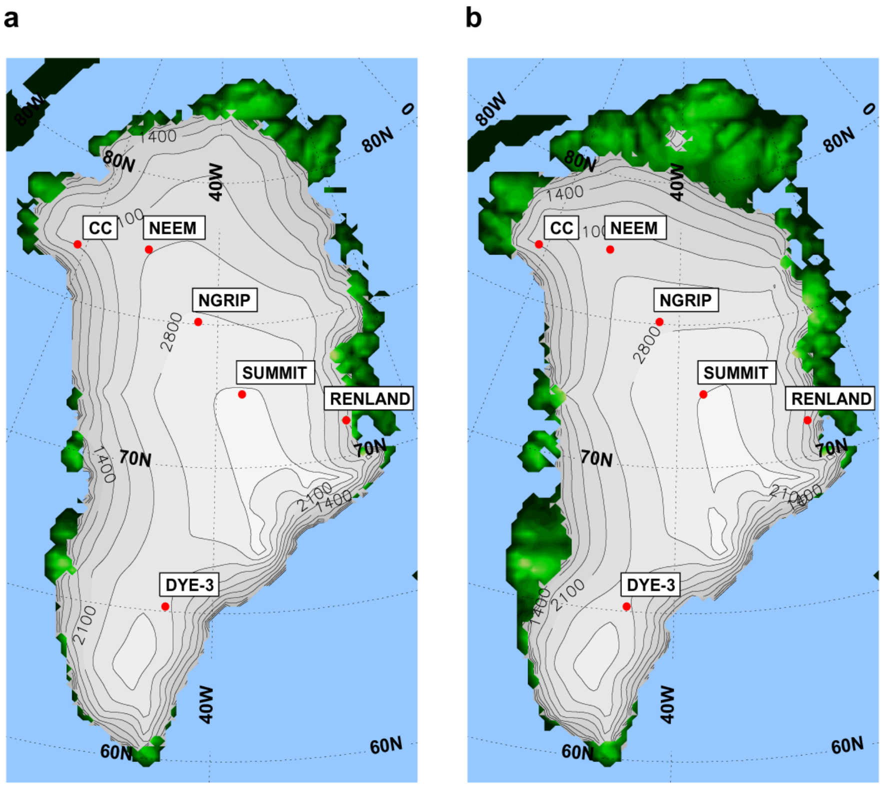

Fig. 11. Simulated minimum GrIS extent for the ensemble member with a maximum GrIS contribution to LIG rise closest to the peak of the probability density plot in Fig. 10a. **(a)** Modern day GrIS extent and **(b)** the minimum GrIS extent during the LIG for a contribution of 1.5 m to LIG sea-level rise.

CPD
8, 2731–2776, 2012

Greenland ice sheet Last Interglacial sea-level contribution

E. J. Stone et al.

Title Page
Abstract | Introduction
Conclusions | References
Tables | Figures
◀| |▶
◀ ▶
Back | Close
Full Screen / Esc
Printer-friendly Version
Interactive Discussion

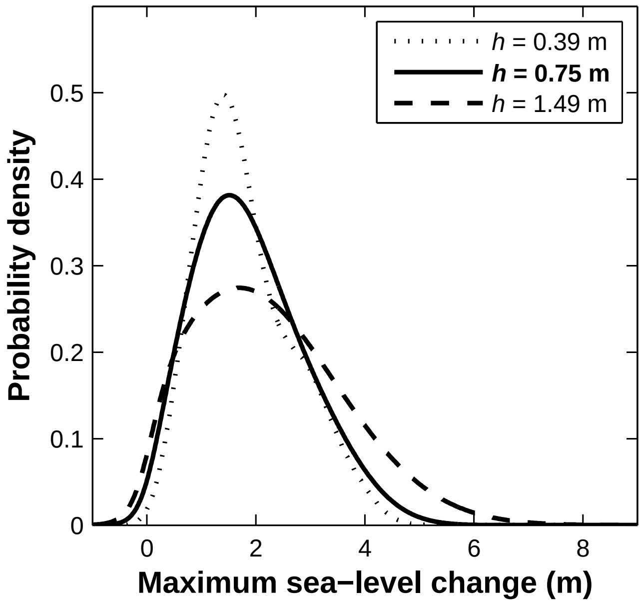

Fig. 12. Sensitivity of the LIG GrIS sea-level contribution probability density function to the Kernel smoothing parameter, *h*. Dotted line: optimal smoothing parameter according to Eq. (13). Solid line: smoothing parameter where modern day observation is 2σ from the ensemble mean (chosen as the most plausible case). Dashed line: smoothing parameter where modern day observation is 1σ from the ensemble mean.

CPD
8, 2731–2776, 2012

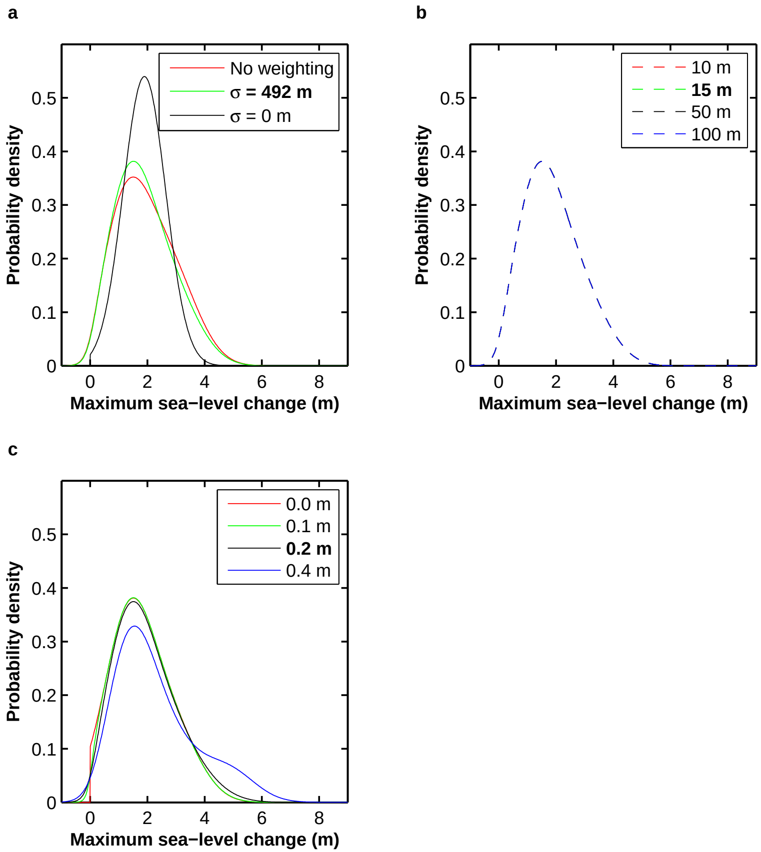

Fig. 13. Sensitivity of the probability density function of the GrIS maximum contribution to sea-level change during the LIG to **(a)** the model error, σ, in Eq. (7), **(b)** observational ice thickness error (τ = 10, 15, 50 and 100 m) from the Bamber et al. dataset (2001) and **(c)** the logistic function given by Eq. (10) (l_w = 0.0, 0.1, 0.2 and 0.4 m). The parameters highlighted in bold are those used for the most plausible case shown in Fig. 10.

CPD
8, 2731–2776, 2012

Greenland ice sheet Last Interglacial sea-level contribution

E. J. Stone et al.

Title Page
Abstract | Introduction
Conclusions | References
Tables | Figures
Back | Close
Full Screen / Esc
Printer-friendly Version
Interactive Discussion

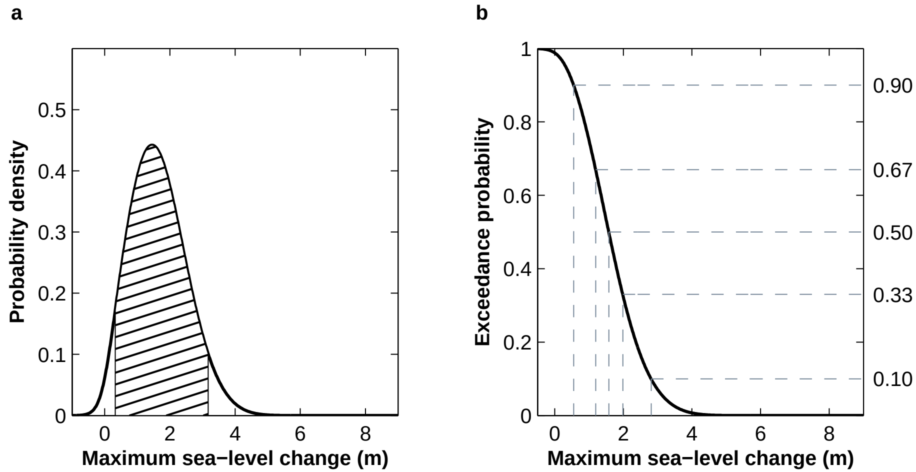

Fig. 14. A probabilistic assessment of the GrIS maximum contribution to sea-level change during the LIG, assuming ice is present throughout the LIG at the NEEM ice core. **(a)** Probability density plot. The hashed region denotes the probability of the contribution from the GrIS being between 0.3 and 3.2 m (90 % confidence interval). **(b)** Exceedance values for the probability distribution. There is a 90 % probability of a GrIS contribution exceeding 0.6 m during the LIG, a 67 % probability of exceeding 1.2 m, a 50 % probability of exceeding 1.6 m, a 33 % probability the contribution exceeded 2.0 m and a 10 % probability it exceeded 2.8 m. An ensemble of 500 simulations weighted according to their skill-score for modern day ice thickness and the presence of ice at NGRIP, Summit and NEEM core locations are used. They are also weighted according to a five dimensional Gaussian fitted to the ice sheet model parameter distributions. The probability density function is constructed using a Kernel density estimator with a window width of 0.75 m.

CPD
8, 2731–2776, 2012